M. Asanishi, T. Takaki and Y. Tomita / Proceedings, AES – ATEMA' 2007 International Conference, Montreal, Canada, August 06 -10, 2007, pp. 195 - 203

ISBN 0-9780479

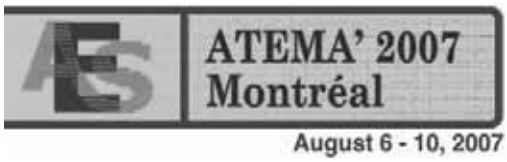

International Conference on Advances and Trends in Engineering Materials and their Applications (AES – ATEMA' 2007)

Polymer Spherulite Growth Simulation during Crystallization by Phase-Field Method

M. Asanishi[1]*, T. Takaki[2] and Y. Tomita[3]

[1] Graduate School of Science and Technology, Kobe University, Kobe, Japan
(Email: asanishi@solid.mech.kobe-u.ac.jp)

[2] Faculty of Maritime Sciences, Kobe University, Kobe, Japan
(Email: takaki@maritime.kobe-u.ac.jp)

[3] Faculty of Engineering, Kobe University, Kobe, Japan
(Email: tomita@mech.kobe-u.ac.jp)

*Corresponding Author

Abstract

The establishment of a coupled numerical model that enables us to simulate spherulite formations and their mechanical behavior continuously for crystalline polymers is our ultimate goal. In this paper, we focus our attention on the formation process of spherulite and the establishment of a spherulite growth model. As a numerical model, the phase-field method is employed here. In the crystallization process of polymers, viscosity and supercooling play an important role in the formation of microstructures. Here, we introduce the viscosity effect as the degree of molecular alignment at the solid-liquid interface. In this model, we employ three order parameters: phase field, which distinguishes between solids or liquids; crystallographic orientation, which characterizes the growth direction of lamellae; and temperature. The effects of viscosity and super cooling on the formed microstructural morphology are investigated by performing a series of numerical simulations.

Keywords

Spherulite, Solidification, Phase-Field Method, Polymer, Lamella

1 Introduction

To enable the wide use of semi-crystalline polymers as structural materials, it is indispensable to establish a numerical model that can predict the macroscopic mechanical

behavior taking their microstructures into consideration. Tomita and Uchida [1], who are members of our group, have proposed a multiscale model relating the micro- to mesoscopic deformation behaviors of semi-crystalline polymers in 2D problems. Furthermore, they have generalized their 2D model to a 3D model in order to represent the 3D structure of lamellae within a spherulite [2]. Although, as mentioned above, sophisticated multiscale models have been developed, the initial spherulite morphology with a radial arrangement of thin lamellae is the input data and is assumed when performing the simulation. The deformation properties of structural polymers are intimately related to the crystallized morphology [3], which changes from a single crystal to the spherulite structure with increasing supercooling [4], and the spherulite is classified into different types depending on the crystallization temperature [5]. Therefore, in order to perform a more comprehensive investigation considering the difference in the microstructure, it is crucial to establish a coupled numerical model of the mechanical properties and the morphological formation.

Surprisingly few numerical studies have so far been carried out on spherulite formation considering the microstructure, although there have been many studies on crystallization kinetics based on the JMAK model [6,7]. Raabe [8] performed a mesoscale simulation of spherulite growth using a cellular automaton. However, the results were limited to the evaluation of crystallization kinetics. Kyu et al. [9, 10] developed phase-field models for crystalline polymers with simple shapes. Very recently, Mattozzi et al. [11] simulated the formation of a spherulite-like structure by a lattice Monte Carlo based a random walk. Although this model includes lengthening, branching and twisting of the lamellae and a visually accurate 3D spherulite structure is reproduced, the model includes many assumptions. Granasy et al. [12] successfully applied a phase-field model for polycrystalline solidification to the simulation of various complex morphologies including spherulite. However, their results were restricted to metallic alloys.

Our ultimate goal is to construct a coupled numerical model that can simulate the morphology formation and the mechanical properties continuously. In this paper, we derive a phase-field model for polymer spherulites by generalizing the model proposed by Granasy et al. [12].

2 Spherulite

Figure 1 shows the hierarchical structures in a polymer. The spherulite shown in (b) is composed of fibrous ribbons growing outward from the center along the *b*-axis and its branching or secondary nucleation. The fibrous ribbon (c) is a two-phase material, consisting of a crystalline lamella and an amorphous layer, that grows with twisting and branching. The lamella has dominant (fold surface) and slower-growing fronts (lateral surface), as illustrated in (d).

Although using the multiscale model for mechanical behavior [2], it is possible to treat all the structures shown in Fig. 1, in this study, we aim to treat the structures shown in Figs. 1 (a) and (b) because of the restriction to 2D. The anisotropic interface energy is closely related to spherulite formation [13]. To simulate the spherulite morphology, the anisotropic growth and branching of lamellae are introduced to the

numerical model presented here.

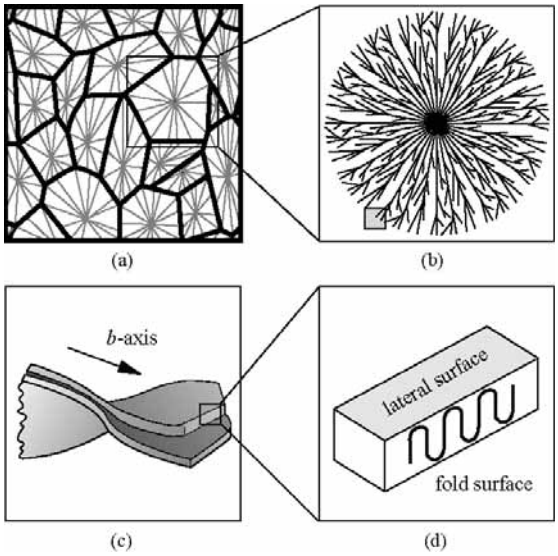

Figure.1 Hierarchical structures in polymer, (a) crystallizing texture, (b) spherulite, (c) twisting lamella and (d) chain folding structure.

3 Phase-Field Model

In order to develop the phase-field model of the super cooling solidification of pure polyethylene, we develop our model from the following free energy functional [14]:

$$F = \int \left[\frac{\alpha(\psi)}{2} |\nabla \phi|^2 + f(\phi, T) + g(\phi) s |\nabla \theta| \right] dA, \quad (1)$$

where ϕ is a phase field that equals zero in the liquid phase and unity in the solid phase, T is temperature, θ is the normalized crystallographic orientation with the interval [0, 1] and $\alpha(\psi)$ is the gradient coefficient depending on the angle ψ between the interface normal and the x-axis. $f(\phi, T)$ is the free energy density in bulk polyethylene, and we employ a normal double well type function:

$$f(\phi, T) = p(\phi) f_{sol}(T) + \left(1 - p(\phi)\right) f_{liq}(T) + W q(\phi), \quad (2)$$

where W is the barrier height, $f_{sol}(T)$ and $f_{liq}(T)$ are the free energy densities inside the solid and liquid respectively, and we use the free energy difference $f_{sol}(T)$-$f_{liq}(T)$=$L(T$-$T_m)/T_m$ as a driving force. $p(\phi)$ and $q(\phi)$ are the energy interpolating function and the double well function, respectively, and we employ $p(\phi) = \phi^3(10\text{-}15\phi\text{+}6\,\phi^2)$ and $q(\phi) = \phi^2(1-\phi^2)$. In Eq. 1, the third term represents the excess free energy density due to the presence of misorientation at the solid-liquid interface and the grain boundary. This term enables us to simulate the branching phenomenon of the fibrous ribbon or secondary nucleation. Here, s is a positive constant that determines the amount of excess energy due to the misorientation. $g(\phi)$ is a monotonically increasing function satisfying $g(1) = 1$ and $g(0) = 0$ to eliminate the misorientation effect in the liquid phase, and we choose $g(\phi) = \phi^3(10\text{-}15\phi\text{+}6\,\phi^2)$.

The interface energy between the fold surface of the lamella and the super cooled melt is almost one order greater than that of the lateral surface [13]. Such a large difference in interface energies is modelled by adopting the following equations for the gradient coefficient:

$$\alpha(\psi) = \begin{cases} \alpha_1(\psi) & (\text{for } 2\pi i/k + \theta_m \le \psi - 2\pi\theta/k \\ & \le 2\pi(i+1)/k + \theta_m) \\ \alpha_2(\psi) & (\text{for } 2\pi i/k - \theta_m \le \psi - 2\pi\theta/k \\ & \le 2\pi i/k + \theta_m), \end{cases} \quad (3)$$

where

$$\alpha_1(\psi) = \frac{\bar{\alpha}}{1+\gamma}\left[1+\gamma\cos\left\{k\left(\psi-\frac{2\pi\theta}{k}\right)\right\}\right] \quad (4)$$

$$\alpha_2(\psi) = \frac{\alpha_1(\theta_m+\theta)}{\cos(\theta_m)}\cos(\psi-\theta). \quad (5)$$

Here, γ is the strength of anisotropy, k is the anisotropic mode, $\bar{\alpha}$ is a constant and θ_m is the first missing orientation angle. If $\gamma < (k^2\text{-}1)$, $\alpha(\psi) = \alpha_1(\psi)$ for all ψ.

The time evolution equations for ϕ, θ and T are obtained as follows:

$$\frac{\partial\phi}{\partial t} = M_\phi\left[-\frac{\partial}{\partial x}\left(\alpha\frac{\partial\alpha}{\partial\psi}\frac{\partial\phi}{\partial y}\right)+\frac{\partial}{\partial y}\left(\alpha\frac{\partial\alpha}{\partial\psi}\frac{\partial\phi}{\partial x}\right) + \nabla\cdot\left(\alpha^2\nabla\phi\right)-\frac{\partial f(\phi,T)}{\partial\phi}-\frac{\partial g(\phi)}{\partial\phi}s|\nabla\theta|\right] \quad (6)$$

$$\frac{\partial\theta}{\partial t} = M_\theta\nabla\cdot\left[g(\phi)s\frac{\nabla\theta}{|\nabla\theta|}\right] \quad (7)$$

$$\frac{\partial T}{\partial t} = \kappa\nabla^2 T + \frac{L}{c}\frac{\partial p(\phi)}{\partial\phi}\frac{\partial\phi}{\partial t}, \quad (8)$$

where t is time, κ is the thermal diffusivity and c is the specific heat. M_ϕ and M_θ are the mobilities of the phase field ϕ and orientation θ, respectively. The mobility M_ϕ determines the crystallization rate and is derived from the kinetic theory [8]. The mobility M_θ is related to the rotational diffusion, which is a function of viscosity. Both mobilities depend on temperature, and the ratio M_θ/M_ϕ determines the degree of second nucleation, or branching.

By considering the 1D equilibrium condition at $T = T_m$ and the steady growth condition, we can obtain the following relations for the interface thickness δ, interface energy σ and the constant interface velocity V:

$$\delta = \frac{\sqrt{2}\alpha(\psi)}{\sqrt{W}}2\tanh^{-1}(1-2\lambda), \quad (9)$$

$$\sigma = \frac{\alpha(\psi)\sqrt{W}}{3\sqrt{2}}+\frac{1}{2}s\Delta\theta, \quad (10)$$

$$V = \frac{6\alpha(\psi)}{\sqrt{2}W}\frac{L(T_m-T)}{T_m}M_\phi, \quad (11)$$

where λ is a minimum value of ϕ in the interface region, such as $\lambda = 0.1$. Although from Eq. 10, the interface energy changes with the misorientation angle $\Delta\theta$, the misorientation dependence on the interface energy σ is eliminated by setting a small value of s. Then, from Eq. 7, the constant s relates only to the rate of reorientation at the solid-liquid interface.

4 Numerical Simulation

First, the effects of super cooling and viscosity on the solidification morphology are investigated by performing the simulation of super cooling solidification. Since, however, the growth rate of the polymer is known to be much slower than that of thermal diffusion, to carry out the super cooling solidification simulation with high accuracy, we need a very large computational time. Therefore, using the hypothetical material constants, we perform a qualitative investigation. Second, in order to perform a more realistic simulation of polymer spherulite formation, we conduct the simulation under an isothermal condition.

We use an explicit finite difference scheme to solve the governing equations. Periodic boundary conditions are applied to a square computational region. The initial distributions of the orientation are random in the range [0, 1] in both the liquid and the nucleus [12].

5 Super-cooling Solidification

5.1 Effects of super-cooling and viscosity

In order to qualitatively investigate the effects of super cooling and viscosity, i.e., the ratio M_θ/M_ϕ, on the morphology. We perform the super cooling solidification simulation using assumed material constants. Here, we use the following parameters: $\Delta x = \Delta y = 10$ nm, $\delta = 4\Delta x = 40$ nm, $\sigma = 0.3$ J/m^2, $\gamma = 0.03$, $\overline{\alpha} = 1.280\times10^{-4}$ (J/m)$^{0.5}$, $W = 9.888\times10^{7}$ J/m^3 and $M_\phi = 6.327$ m^3/Js. The computational domain is set to be 4×4 μm = 400 Δx×400 Δy (400×400 grid).

Figure 2 indicates the effect of the driving force, or super cooling, on the morphology for $M_\theta/M_\phi = 10$. Here, Δ is the degree of normalized super cooling defined by $(T_m - T_i)/T_m$. In the case of small Δ, the crystal morphology becomes dendritic in shape, as shown in Fig. 2 (a), because of the diffusion-controlled process. In the case of large Δ, it is observed that the crystal is circular, as can been seen in Figs. 2 (b) and (c). Furthermore, from Fig. 2, we can see finer microstructures with increasing driving force, because the crystallization rate becomes faster than the rotational one.

Figure 3 shows the effect of the ratio M_θ/M_ϕ on the morphology for $\Delta = 1.0$. It is observed that thicker and longer crystals grow within spherulite with increasing M_θ/M_ϕ. In other words, when M_θ/M_ϕ becomes smaller than a certain critical point, the growing front has difficulties in incorporating the same crystallographic orientation and generates a second nucleation. The disordered distributions of the crystallographic orientation along the growing front cause the formation of a circular morphology, as shown in Fig. 3 (a), regardless of the anisotropic interface energy.

It can be concluded from the above numerical results that the shapes of the morphology and microstructures within the spherulite are largely dependent on the ratio of the crystallization rate to the rotational one, i.e., the ratio M_θ/M_ϕ.

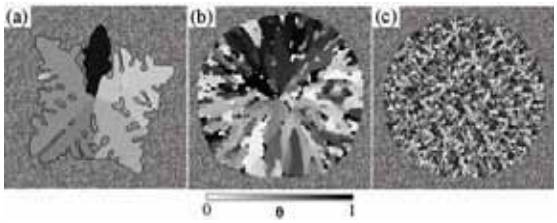

Figure.2 Effects of driving force on morphology and microstructure for Δ = (a) 0.8 (t = 0.32 μsec), (b) 0.9 (t = 0.19 μsec) and (c) 1.0 (t = 0.15 μsec).

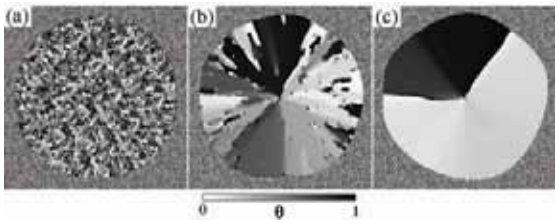

Figure.3 Effects of mobility ratio on morphology and microstructure at t = 0.15 μsec for M_θ/M_ϕ = (a) 100, (b) 200 and (c) 300.

5.2 Polymer spherulite

In this section, we discuss the typical spherulite formation of the polymer, as shown in Fig. 4. Experimental studies [15] have shown that the early stage of polymer spherulite growth is the formation of a bundle of lamellae, as shown in Fig. 4. The growth fronts that induce secondary nucleation lamellae split and branch. The branching of lamellae brings about the conversion into ribbon-shaped crystals, such as

those in Fig. 4. The morphology eventually becomes that of the spherulite by the space being filled with the branched lamellae.

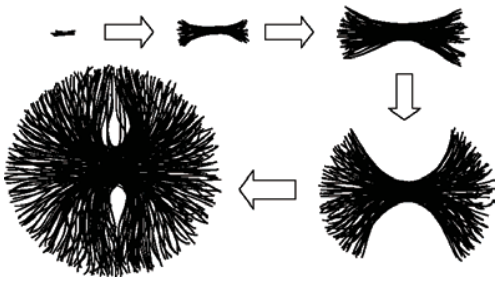

Figure.4 Spherulite growth sequence.

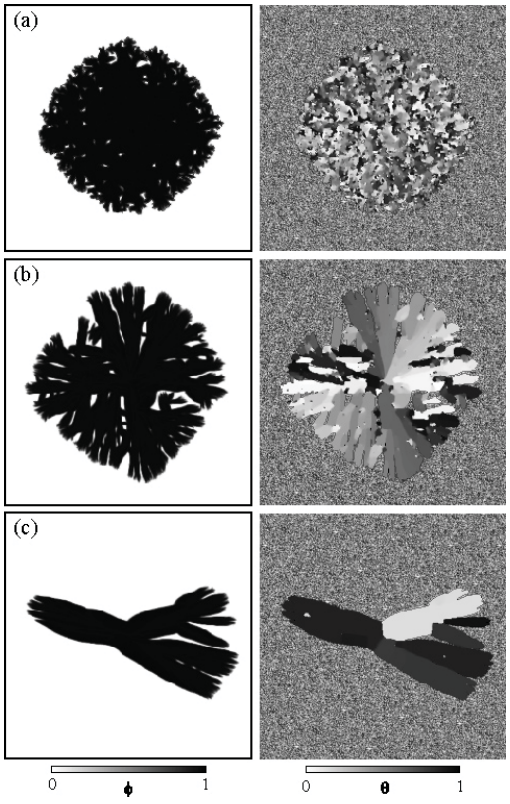

Figure.5 Calculated morphologies with high interface anisotropy for M_θ/M_ϕ = (a) 100, (b) 200 and (c) 300. The left diagram is the phase field, and the right is orientation.

Figure 5 illustrates the crystal growth in the case of the high anisotropic interface energy of $\gamma = 0.8$. The anisotropic mode is employed as $k = 2$ to represent the lamellae growth. As shown in Fig. 5, when a tip of a growing lamella absorbs the orientational defects into the growth front, it changes its growing direction. Furthermore, it can be observed that as the ratio M_θ/M_ϕ decreases, the branching at the liquid-solid interface occurs more frequently and results in the polycrystalline morphology with fine grains.

On the basis of the surface nucleation model [13] proposed by Hoffman, the growth mode of the polymer is categorized into three regimes, i.e., regimes I, II and III. Each regime is determined by the ratio of the secondary nucleation rate to the crystal growth rate at the chain folding surface. With increasing rate, a transition from regime I to regime III occurs. Under the condition in regime I, the lamellae preferentially grow as shown in Fig. 5 (c). In regime III, a lot of secondary nuclei are generated and disordered crystal growth is observed, as shown in Fig. 5 (a). Although it seems that the condition shown in Fig. 5 (b) is that of regime II, the calculated morphology is different from that shown in Fig. 4. Next, we perform the same simulation for M_θ/M_ϕ = 230, but the computational domain is changed to 6×6 μm (600×600 grid). In the early growth process, the crystal is thread- shaped, as shown in Fig. 6. Secondary nucleation brings about splitting and branching lamellae, and finally the spherulite shown in Fig. 4 is formed. It is concluded that the formation process of this polymer spherulite requires both the needle-shaped lamellae growth and the secondary nucleation or, branching.

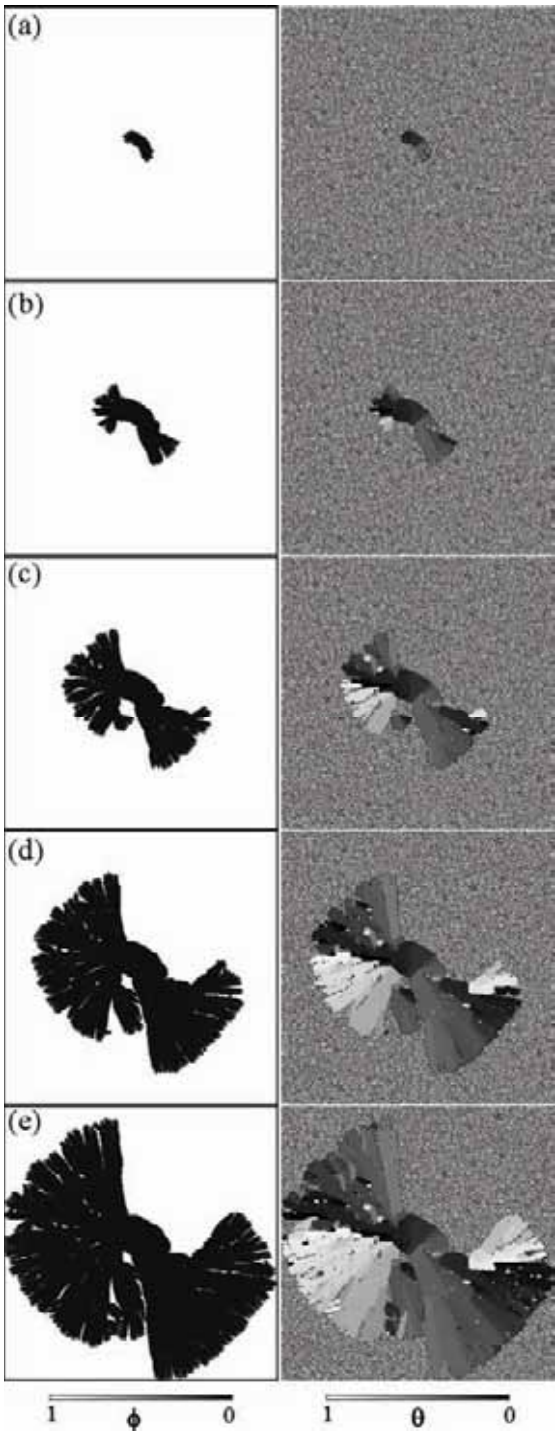

Figure.6 The occurrence of spherulite with branching lamellae at t = (a) 0.036, (b) 0.99, (c) 0.144, (d) 0.198 and (e) 0.252 μsec.

6 Isothermal Solidification

In the previous section, the spherulite formation simulation of the supercooling melt is performed using the assumed parameters to qualitatively investigate the effects of the solidification conditions on the formed morphology. In this section, in order to enable a more realistic simulation of the spherulite formation of the polymer, we perform the simulation under isothermal conditions in which the experimental studies were carried out [5]. By assuming isothermal conditions, it is not necessary to solve Eq. 8, and the computational effort can be reduced. We use the following parameters: σ = 0.1 J/m^2, Δx = Δy = 10 nm, $\delta = 4\Delta x$ = 40 nm, $\overline{\alpha}$ = 7.390×10^{-5} (J/m)$^{0.5}$, W = 3.296×10^7 J/m^3, T_m = 418.7 K [13], and M_ϕ = 4.087×10^{-7} m^3/sJ. The value of M_ϕ is determined by assuming V = 0.1 μm/s [8] and T = 412 K from Eq. 11. Here, the numerical results for isotropic interface energy are indicated.

Figure. 7 shows the effect of the mobility ratio on the morphology and microstructure. It is found that we obtain equivalent results to those shown in Fig. 3.

Figure 8 shows a time sequence showing the growth of the number of spherulites. The domain is set to be 12×12 μm (1200×1200 grid) and M_θ/M_ϕ = 60. Twelve nuclei are generated simultaneously initially (site saturated nucleation model). All nuclei grow and impinge on the neighbor spherulites. Finally, the whole space is filled with the spherulite morphologies. Although these results are for the isotropic interface energy, the

obtained morphology is very similar to experimentally observed results, e.g., Fig. 1 of Ref. [16].

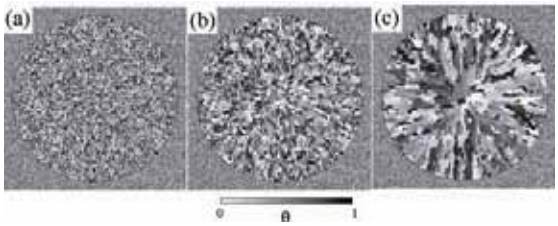

Figure.7 Spherulite morphology at t = 25 s for M_θ/M_ϕ = (a) 20, (b) 40 and (c) 60

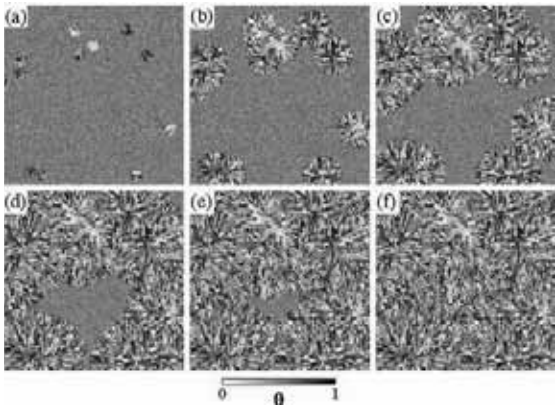

Figure.8 Spherulite growth sequences t = (a) 5, (b) 15, (c) 25, (d) 35, (e) 45 and (f) 55 s.

7 Conclusions

A phase-field model for polymer spherulite growth has been established by generalizing the model proposed by Granasy et al. [12]. By performing a series of simulations, it is clarified that the driving force of solid-liquid interface migration and the viscosity, which control the crystallization and rotation of crystal orientation, are dominant factors that determine the morphology and microstructure. Furthermore, it is confirmed that, in order to reproduce the typical spherulite growth process, a high anisotropy, which creates the needle-shaped crystals and the secondary nucleation are required. Finally, a simulation under the isothermal condition was carried out using realistic material parameters of the polymer, which provides a spherulite morphology similar to experimentally observed results.

Acknowledgments

This research was partially supported by the Ministry of Education, Culture, Sports, Science and Technology Grant-in-Aid for Scientific Research (B), 18360061, 2007.

References

[1] Tomita, Y. and Uchida, M. (2005) Computational Characterization of Micro- to Mesoscopic Deformation Behavior of Semicrystalline Polymer, *Int. J. Mech. Sci.*, 47 *(4/5)*, 687 – 700.

[2] Tomita, Y. and Uchida, M. (2005) Computational Characterization and Evaluation of Deformation Behavior of Spherulite of High Density Polyethylene in Mesoscale Domain, *Computer Modeling in Engineering & Sciences,* 10 *(3)*, 239 - 248.

[3] Way, J. L., Atkinson, J. R. and Nutting, J., (1974) The effect of spherulite size on the fracture morphology of polypropylene, *J. Mater. Sci., 9 (2)*, 293 - 299.

[4] Magill, J. H. and Plazek, D. J. (1967) Physical Properties of Aromatic Hydrocarbons. II. Solidification Behavior of 1,3,5-Tri-α-Naphthylbenzene*, *J. Chem. Phys.,* 46 *(10)*, 3757 - 3769.

[5] Norton, D. R. and Keller, A. (1984) The spherulitic and lamellar morphology of melt-crystallized isotactic polypropylene, *Polymer,* 26 *(5)*, 704 - 716.

[6] Koscher, E. and Fulchiron, R. (2002) Influence of shear on polypropylene crystallization: morphology development

and kinetics, *Polymer,* 43 *(25)*, 6931 - 6942.

[7] Hieber, C. A. (1995) Correlations for yhe quiescent crystallization kinetics of isotactic polypropylene and poly(ethylene terephthalate, *Polymer,* 36 *(7)*, 1455 - 1467.

[8] Raabe, D. (2004) Mesoscale simulation of spherulite growth during polymer crystallization by use of a cellular automaton, *Acta. Mater*., 52 *(9)*, 2653 - 2664.

[9] Kyu, T., Mehta, R. and Chiu, H. –W. (2000) Spatiotemporal growth of faceted and curved single crystals, *Phys. Rev. E*, 61 *(4)*, 4161 - 4170.

[10] Metha, R., Keawwattana, W. and Kyu, T. (2004) Growth dynamics of isotactic polypropylene single crystals during isothermal crystallization from a miscible polymeric solvent, *J. Chem. Phys.,* 120 *(8)*, 4024 - 4031.

[11] Mattozzi, A., Serralunga, P., Hedenqvist, M. S. and Gedde, U. W. (2006) Mesoscale modelling of penetrant diffusion in computer-generated polyethylene–spherulite-like structures, *Polymer,* 47 *(15)*, 5588 - 5595.

[12] Granasy, L., Pusztaiet, T., Tegze, G., Warren, J. A. and Douglas, J. F. (2005) Growth and form of spherulites, *Phys. Rev. E,* 72 *(1)*, 011605.

[13] Hoffman, J. D. and Miller, R. J. (1997) Kinetics of crystallization from the melt and chain folding in polyethylene fractions revisited: theory and experimant, *Polymer,* 38 *(13)*, 3135 - 3212.

[14] Kobayashi, R., Warren, J. A. and Carter, W. C. (2000) A continuum model of grain boundaries, *Physica D,* 140 *(1-2)*, 141 - 150.

[15] Lei, Y. –G., Chan, C. –M., Wang, Y., Ng, K. –M., Jiang, Y. and Lin, L. (2003) Growth process of homogeneously and heterogeneously nucleated spherulites as observed by atomic force microscopy, *Polymer,* 44 *(16)*, 4673 - 4679.

[16] Magill, H. (2001) Spherulites: A personal perspective*, *J. Mater. Sci.*, 36 *(13)*, 3143 – 3164.